Dimensional accuracy and impact resistance of 3D printed clay reinforced with scrap polymer powder

Dimensional accuracy and impact resistance of 3D printed clay reinforced with scrap polymer powder

Abstract

Purpose The purpose of this paper is to give an insight into relevant aspects of 3D printing of clay paste enhanced with scrap polymer powder which have not been investigated by previous studies. Specifically, the geometrical features of the deposited lines, dimensional accuracy of benchmarks and mechanical properties of printed parts are investigated.

Design/methodology/approach

Firstly, the 3D printer is used to deposit lines of the paste under various combinations of material composition and process parameters. 3D scanning is used to measure their dimensional and geometrical errors. The results are elaborated through statistics to highlight the role of material and processing conditions. Then, four benchmark parts are printed using materials with different percentages of polymer powder. The parts are scanned after each step of the post-processing to quantify the effects of printing, drying and melting on dimensional accuracy. Finally, drop weight tests are carried out to investigate the impact resistance of specimens with different powder contents.

Findings

It is found that the quality of deposition varies with the printing speed, nozzle acceleration and material composition. Also, significant differences are observed at the ends of the lines. Materials with 10 wt% and 40 wt% of powder exhibit relevant shape variations due to the separation of phases.

Accuracy analyses show significant deformations of parts at the green state due to material weight. This effect is more pronounced for higher powder contents. On the other hand, the polymer reduces shrinkage during drying.

Further, the impact test results showed that the polymer caused a large increase in impact resistance as compared to pure clay. Nonetheless, a decrease is observed for 40 wt% due to the higher amount of porosities.

Research implications

The results of this study advance the knowledge on the 3D printing of clay paste reinforced with a scrap polymer powder. This offers a new opportunity to reuse leftover powders from powder bed fusion processes. The findings presented here are expected to foster the adoption of this technique reducing the amount of waste powder disposed of by additive manufacturing companies.

Originality/value

This study offers some important insights into the relations between process conditions and the geometry of the deposited lines. This is of practical relevance to toolpath planning.

The dimensional analyses allow for understanding the role of each post-processing step on the dimensional error. Also, the comparison with previous findings highlights the role of part dimensions.

The present research explores, for the first time, the impact resistance of parts produced by this technology. The observed enhancement of this property with respect to pure clay may open new opportunities for the application of this manufacturing process.

Keywords: Material Extrusion, Clay, Recycling, Additive Manufacturing, Polyamide

---

List of acronyms

1. Introduction

The Additive Manufacturing (AM) of polymeric powders dates back to 1980, when Carl R. Deckard patented the Laser Powder Bed Fusion (LPBF) process, originally termed Selective Laser Sintering (SLS) [1]. LPBF is still one of the most widespread Three-Dimensional Printing (3DP) technologies, with numerous applications in industry and research [2–4]. In recent years, several Powder Bed Fusion (PBF) technologies to transform polymer materials have been introduced besides LPBF [5], such as High-Speed Sintering (HSS) [6, 7], Selective Inhibition Sintering (SIS) [8, 9] and Multi Jet Fusion (MJF) [10–12]. These processes allow for a dramatic reduction of production time if compared with LPBF and foster the adoption of polymer PBF on a large scale. Accordingly, a

constantly increasing trend in the industrial applications of these technologies has been observed in recent years [13, 14].

The rapid spread of AM technologies requires a critical analysis of their environmental impacts [15–17]. Specifically, PBF processes suffer from an intrinsic limitation related to feedstock material. In fact, in all the PBF processes mentioned above, the non-transformed powder undergoes thermal ageing [18–21]. Ageing determines a modification of powder properties which in turn may lead to a drop in mechanical performances and to non-correct sintering of the part [22, 23]. As a consequence, the non-transformed material has to be mixed with virgin polymer for reusing [24, 25]. This means that a considerable amount of powder must be disposed of at the end of each print. The management of this waste is thus a key topic as far as the sustainability of polymer PBF is concerned.

The primary method that has been used in literature is reusing the scrap powder to produce filament for Fused Filament Fabrication (FFF). This strategy has been first adopted by Mägi et al., who characterised the mechanical properties of filament produced by leftover Polyamide 12 (PA12) from LPBF. In order to tune the mechanical properties, the authors mixed the scrap powder with Thermoplastic Polyurethane (TPU) pellet and aramid fibres [26]. Kumar and Aleksander presented a detailed investigation into the properties of filament produced by reinforcing PA12 powder with various percentages of Tungsten Carbide (WC) [27]. Similar studies were proposed by Wang et al. [28] and Uddin et al. [29], who used milled Carbon Fibres (mCF) and Magnesium (Mg) particles, respectively, to reinforce PA12. A comparison between PA12 filament obtained from the virgin pellet and scrap powder was presented by Feng et al. [30], who highlighted the influence of the printing speed on mechanical properties. These studies demonstrated the opportunity to use FFF to recycle scrap powder from PBF. Nevertheless, this method suffers from serious drawbacks due to the need for producing the feedstock filament. Firstly, the powder must undergo full remelting, which might modify its physical and thermal properties [31, 32]. Moreover, strict control of the filament diameter is necessary since the

FFF process is extremely sensitive to filament diameter [33, 34]. This problem is exacerbated by the limited performances of desktop filament extruders, which limit the opportunities for distributed recycling [35].

A different method for recycling scrap PA12 powders through clay Material Extrusion Additive Manufacturing (MEAM) has been recently proposed [36]. The AM of clay is an increasingly important area of research due to the appealing properties of these materials [37, 38]. Accordingly, numerous potential applications of 3D-printed clay parts have been shown in the literature [39, 40]. MEAM is arguably the most widespread technique used for clay AM and can be performed using various technological solutions [41]. Over the last few years, an increasing interest in low-cost desktop MEAM machines can be observed, easing the adoption of these technologies by private users and Small and Medium Enterprises (SMEs) [42, 43].

To date, the study presented in [36] has been the only application of clay MEAM for the recycling of scrap polymer from PBF. That paper demonstrated the feasibility of the process and the upper limit of the polymer concentration in the clay paste. Also, it was shown that the addition of scrap powder mitigates shrinkage in the drying phase, which is the most influential on part accuracy [36]. Nevertheless, a number of questions regarding this process remain to be addressed. Firstly, [36] performed test extrusions by measuring the mass of paste extruded in a given time span. This method does not allow for understanding the actual dimensional stability of the deposited line. Also, the authors highlighted the need for further studies on geometrical accuracy when scaling up the benchmarks [36]. Finally, no information on the mechanical properties of the manufactured parts was given. The latter point is especially important to determine the actual fields of applicability of this technology. Specifically, the impact resistance of clay-based material is often a critical aspect to be considered [44]. Several studies investigated the impact resistance of polymer-clay nanocomposites [45, 46]. These studies showed that the addition of clay dispersions to a polymer matrix leads to little or no loss in impact toughness [47, 48]. Nonetheless, the final behaviour strongly depends on the specific polymer and

clay used in the mixture [49, 50]. To date, no study investigated the impact behaviour of clay reinforced by the addition of polyamide.

The aim of the present study is to fill the gaps mentioned above through an experimental investigation into the MEAM of clay paste enhanced by scrap powder. To this end, the accuracy of the deposited lines is investigated by means of 3D scanning. Then, the impact resistance of parts with different powder percentages is measured through drop weight impact tests.

2. Materials and methods

2.1. Equipment

The printing processes were carried out using the equipment presented in [36]. The frame of a Replicator 2X FFF machine was used. The original motherboard of the printer was replaced with a RAMPS 1.4 - Arduino Mega 2560. This allows for processing custom G-Code using Marlyn 1.9 firmware, which is necessary to adapt the printer to clay printing [36]. Clay extrusion was carried out through a two-step solution. Specifically, namely a Stoneflower ceramic 3D printing kit 2.1 was used. In the first stage, a mechanic piston feeds the clay paste through a hose to the second step. Here, an Archimedes' screw extrudes the clay paste through the deposition nozzle [41]. The secondary extrusion system was mounted on the X-carriage of the machine in place of the original filament extruder. The custom 3D printed parts made available in [36] were used to adapt the kit to the original printer frame. Figure 1 shows a picture of the machine.

2.2. Material

The extruded paste was prepared by mixing clay with scrap PA12 powder. The latter was collected from the leftover powder of an HP MJF 4200 machine operating in *balanced* mode [51]. As discussed in [36], using the equipment detailed above, the mass percentage of PA12 cannot exceed 40% to prevent clogging of the extruder. Accordingly, tests with 10%, 20%, 30% and 40% of PA12 were carried out. 30% of water was included in all the mixtures.

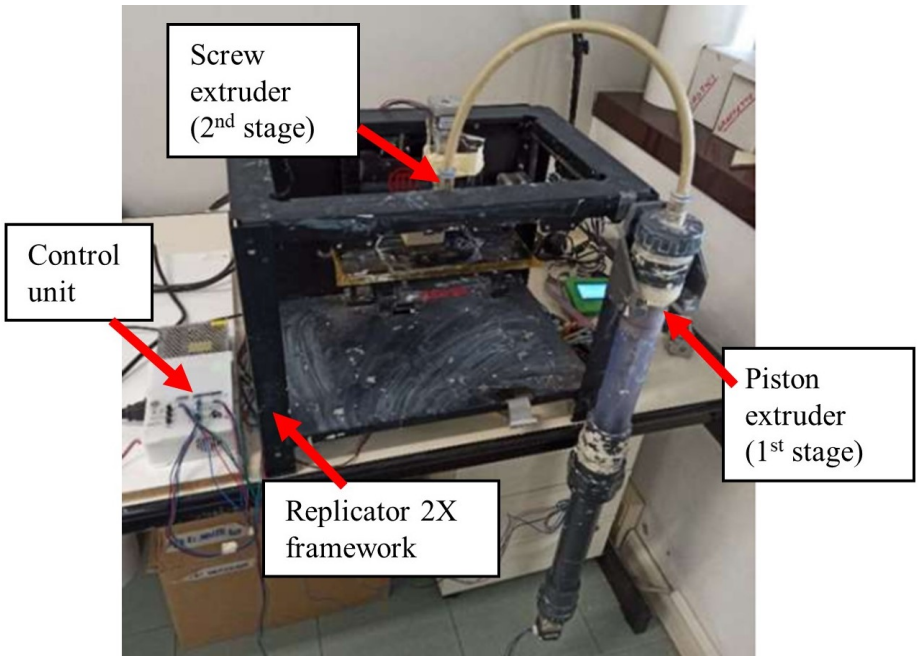

Figure 1: Equipment used for clay paste extrusion. Figure by authors.

2.3. Deposition tests

To investigate the quality of the deposition process, single lines of the clay paste were extruded using different parameters and then digitalised through a 3D scanner. Lines measured 180 mm and were oriented along the X-axis of the machine. A nozzle of 1 mm in diameter was used for the deposition. The experiment was designed by varying the nozzle acceleration (a_n), deposition speed (v_n) and PA12 mass percentage according to the values reported in Table 1. The deposition parameters that were not varied in the experiment are summarised in Table 2. A full-factorial Design Of Experiment (DOE) was used [52]. Three lines distanced by 13 mm were printed for each testing condition. Two repetitions of the experiment were carried out, resulting in 144 measured lines.

Lines were printed on a glass plate. After printing, the plate with the deposited lines was scanned by means of a Faro CAM2 Edge ScanArm HD [36, 53].

Table 1: Parameters varied in the experiment. Table by authors.

Parameter	Levels	Values	Unit of measurement
Nozzle acceleration (a_n)	2	(150, 800)	$\frac{mm}{s^2}$
Nozzle speed (v_n)	3	(30,60,90)	$\frac{mm}{s}$
PA12 percentage	4	(10,20,30,40)	$wt\%$

Table 2: Deposition parameters of single lines. Table by authors.

Parameter	Value	Unit of measurement
Layer Height	0.6	mm
Extrusion Width	1.2	mm
Extrusion Multiplier	0.56	-
Retraction	0.01	mm
Extra Restart Distance	0.1	mm
Vertical Lift	1	mm
Retraction Speed	50	mm/s
Coasting Distance	0.2	mm
Wipe Distance	1	mm

The scanner was controlled through the software Geomagic Studio by 3D System. The acquired point cloud was cleaned to isolate the deposited lines. The *wrap* function of Geomagic was then used to create a polygonal mesh from the point cloud. To quantify the accuracy of the extrusion, the scan of each line was divided into 5 segments with a length of 36 mm. Each segment was fitted to a cylinder through the *best-fit* function of Geomagic, as shown in Figure 2. This function returns the average diameter and the standard deviation of points. These values were then used for statistical analyses. The influence of the process parameters was investigated by means of Analysis Of Variance (ANOVA). Specifically, the General Linear Model (GLM) approach was applied using the statistical software Minitab [52, 54].

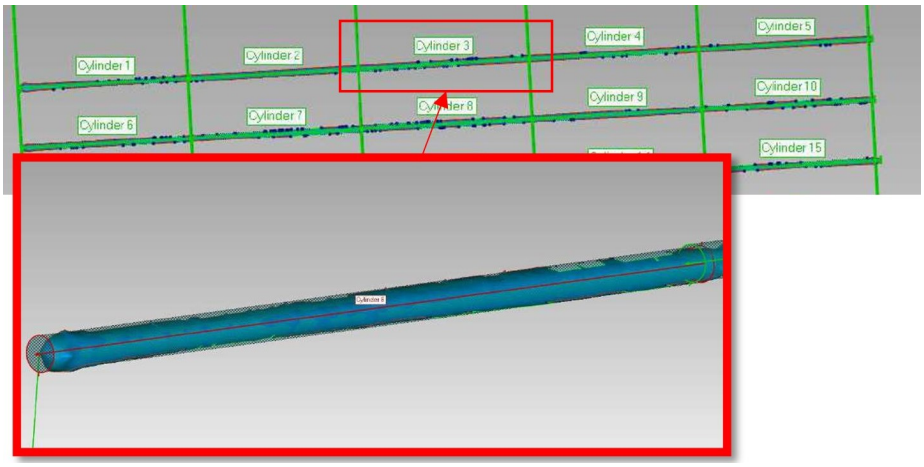

Figure 2: Fitting of cylinders to segments of the scanned lines. Figure by authors.

2.4. Accuracy tests

The accuracy tests were performed on the same geometries proposed by [36], namely a cube, a cylinder and a hollow cylinder. The parts have been scaled up to investigate the accuracy of larger dimensions. Also, a hollow cube was added to the experiment to observe the behaviour of planar thin walls. The specimens are shown in Figure 3, which highlights the nomenclature of dimensions along the X, Y and Z direction. The numerical values of these dimensions are made explicit in the figure caption.

The parts were printed using four mixtures with, respectively, 10%, 20%, 30% and 40% of PA12 powder. Three replicas of each specimen were printed for each material composition, resulting in 48 total specimens. The parameters used for printing are summarised in Table 3.

The build platform was covered with a Polyethylene (PE) film to ease the removal at the end of the printing process. Immediately after printing, the specimens were scanned by means of the FARO CAM2 Edge ScanArm HD 3D scanner mentioned in section 2.3.

After this acquisition, the parts were dried according to the method described by [36]. This method consisted of two phases, namely the conditioning

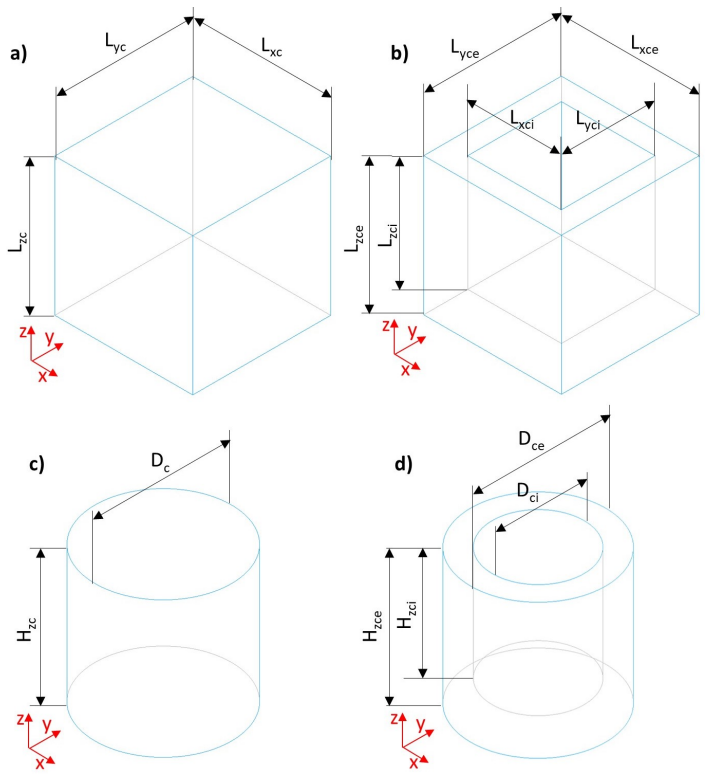

Figure 3: Specimens used for accuracy tests: a) Full cube ($L_{xc} = L_{yc} = L_{zc} = 50\,mm$), b) hollow cube ($L_{xce} = L_{yce} = L_{zce} = 50\,mm$, $L_{xci} = L_{yci} = 34\,mm$, $L_{zci} = 42\,mm$), c) full cylinder ($D_c = H_{zc} = 50\,mm$), d) hollow cylinder ($D_{ce} = H_{zce} = 50\,mm$, $D_{ci} = 34\,mm$, $H_{zci} = 42\,mm$). Figure by authors.

and the drying phases. In the first phase, the part is maintained in an environment with humidity between 85% and 98%. During this phase, microwaves are used to warm the internal part of the component between $27°C$ and $35°C$ so as to promote the migration of water towards external surfaces. In the second phase, the temperature of the chamber is raised to $70°C$ for 120 minutes while maintaining a high humidity of the chamber. Finally, additional 60 minutes at $85°C$ are used to complete drying [36]. After drying, a second scanning of the parts was performed.

Finally, the parts were put in an oven at $200°C$ to melt the polymer powder [36]. The third scan of parts was taken at the end of this treatment.

Table 3: Deposition parameters of impact specimens. Table by authors.

Parameter	Value	Unit of measurement
Layer Height	0.6	mm
Extrusion Width	2	mm
Deposition Speed	45	$\frac{mm}{s}$
Extrusion Multiplier	0.57	-
Infill density	100	%
Infill angle	± 45	$^\circ$
Infill/contour overlap	35	%

The scans were analysed by using the software Geomagic Studio by 3D System to inspect the geometrical accuracy. Specifically, the dimensions shown in Figure 3 were measured at each stage of the post-processing cycle. The measurements were used to calculate the percentage deviation of each dimension with respect to the previous stage ($E_{r\%}$) and to the nominal value ($E_{a\%}$) [36].

2.5. Impact tests

Drop weight impact tests were performed according to the ASTM D7136 [55]. The specimen used for testing is a parallelepiped measuring $110\,mm \times 160\,mm \times 11\,mm$. These dimensions are higher than those prescribed in the standard in order to account for dimensional shrinkage occurring during drying and heat treatment [36]. A nozzle of 2 mm in diameter was used for printing specimens. The hatching was performed through parallel lines oriented at $\pm 45^\circ$. The infill parameters used for printing are reported in Table 4. Other process parameters are as in Table 2.

Specimens with 0 wt%, 10 wt%, 20 wt%, 30 wt% and 40 wt% of scrap PA12 powder were tested. For each composition, 5 replications of the test were carried out.

After printing, specimens were dried and heat treated as described in Section 2.3 and [36].

Table 4: Deposition parameters of impact specimens. Table by authors.

Parameter	Value	Unit of measurement
Layer Height	1.2	mm
Extrusion Width	2	mm
Deposition Speed	30	$\frac{mm}{s}$
Extrusion Multiplier	0.57	-
Infill density	100	%
Infill/contour overlap	35	%

Figure 4 shows the equipment used for drop weight impact tests. The machine is equipped with a laser cell (shown in Figure 4 b) to measure the velocity of the impactor before and after the impact. The signal was acquired at 100 kHz. Figure 4 c) shows the impactor used for testing, which was a semi-sphere with a diameter of 1 inch (i.e. 25.4 mm). The impactor was made of stainless steel with a hardness of 61 HRC. The mass of the impactor and sledge was equal to 1.530 kg. A piezoelectric load cell PCB 208C05 was mounted on the impactor to measure the force during the impact. NI-DAQmx by National Instruments®and Data Acquisition Toolbox™Support Package by MATLAB®were used for acquiring the signal. The acquisition frequency was equal to 100 kHz.

After preliminary tests, the drop height of the impactor was set to 750 mm to ensure the breaking of all the specimens. Impact force and adsorbed energy were calculated according to [55].

3. Results and discussion

3.1. Deposition tests

As mentioned in section 2.3, the average value and standard deviation of the best-fit cylinder of each extrusion segment were used for analyses. The average value of the cylinder diameter provides information about the amount of deposited clay paste, while the standard deviation values quantify the geometrical consistency of the extruded tracks.

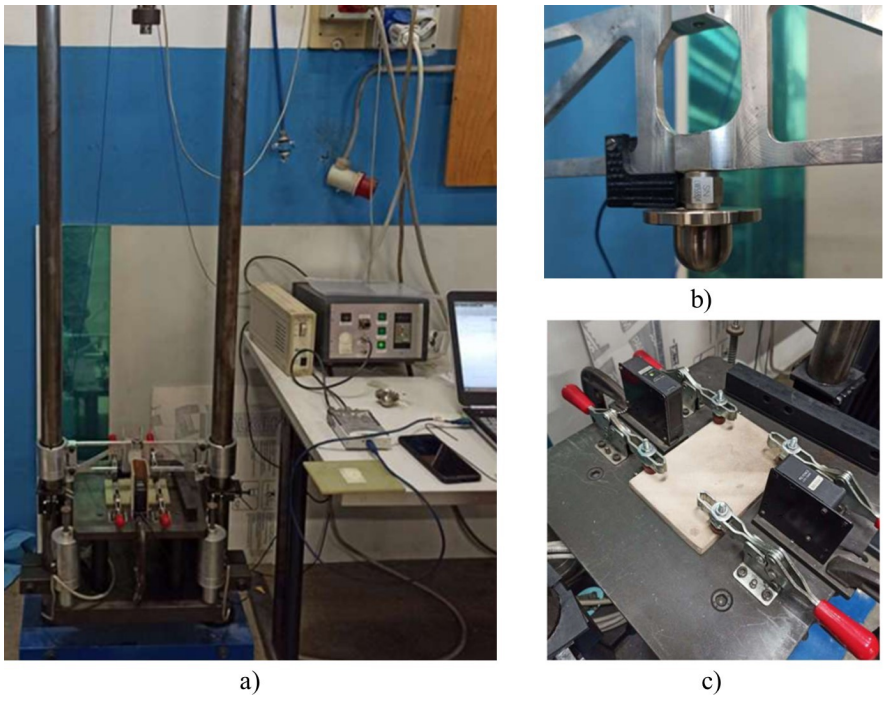

Figure 4: a) Equipment used for drop weight impact tests, b) detail view of the impactor, c) detail view of the specimen clamping and optical cells. Figure by authors.

3.1.1. Average diameter

Table 5 reports the Degrees of Freedom (DF), adjusted Sum of Squares (SS), adjusted Means Square (MS), F-value and p-value of each parameter obtained by means of ANOVA.

The adjusted R^2 of the GLM was equal to 73.02%. Figure 5 shows the normal probability plot for standardised residuals. A Kolmogorov-Smirnov (KS) test for normality was performed on the standardised residuals [56, 57]. The KS test returned a p-value equal to 0.071 and a KS coefficient equal to 0.045. This allows rejecting the hypothesis of non-normal distribution, thus validating the results of ANOVA [52].

The results in Table 5 show that the p-value of v_n is higher than 0.05, i.e. the deposition speed has no effect on the average diameter of the deposited line. This result confirms that the extrusion process is stable in the investigated

Table 5: ANOVA on the average diameter of the best-fitting cylinder

Parameter	DF	Adj SS	Adj. MS	F-value	P-value
v_n	2	2.37×10^{-2}	1.18×10^{-2}	6.10×10^{-1}	5.46×10^{-1}
wt% PA12	3	1.35×10	4.51	2.31×10^{2}	0.00
Position	4	2.93×10^{-1}	7.32×10^{-2}	3.74×10	5.00×10^{-3}
a_n	1	5.35	5.35×10	2.74×10^{2}	0.00

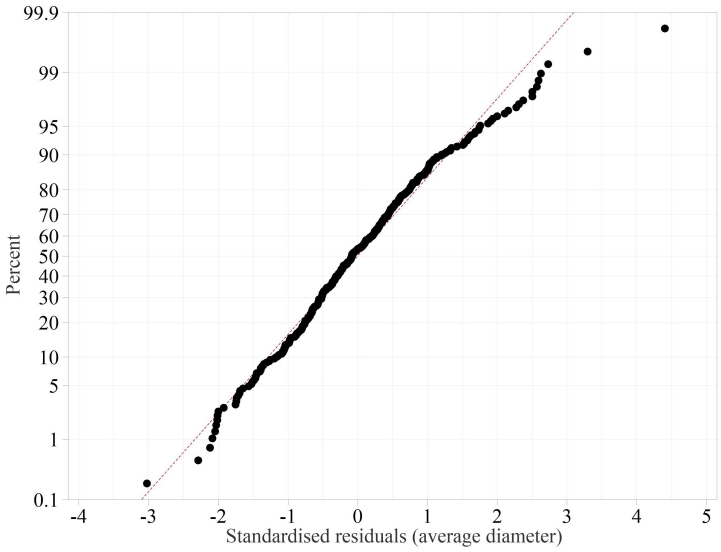

Figure 5: Normal probability plot for standardised residuals of ANOVA on the average diameter. Figure by authors.

range of velocity due to good coordination between the stepper motors of the two extrusion phases. On the other hand, the process is highly sensitive to the weight percentage of PA12, whose F-value is equal to 231. Particularly, the main effects plot in Figure 6 shows that the average diameter in the case of 10 wt% paste is significantly higher than the one observed in all the other cases.

This result is partially explained by the findings of [36], who showed that the mass flow decreases when the PA12 percentage increases. Nevertheless, other factors need to be considered to justify the observed difference. A possible explanation is that the higher percentage of clay intensifies the swelling phenomenon

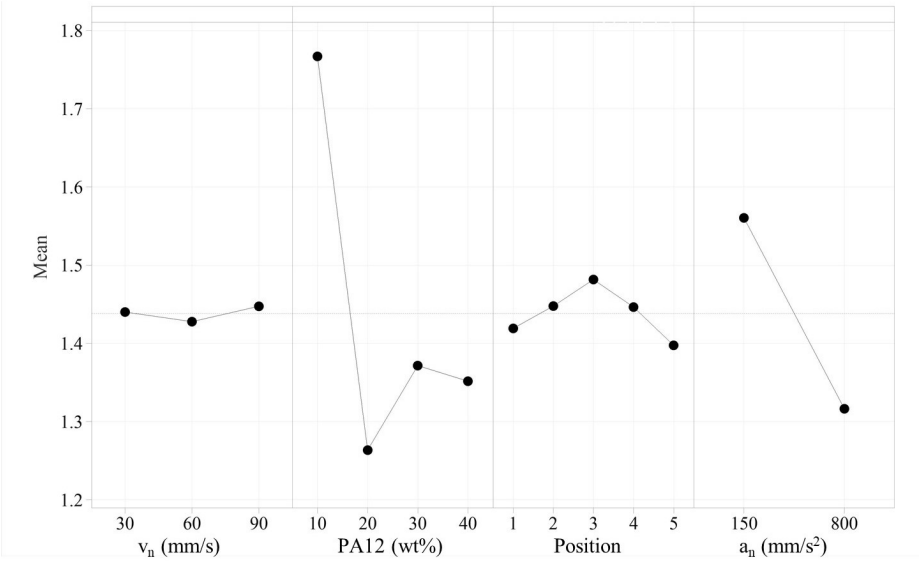

Figure 6: Main effects plot for average diameter. Figure by authors.

due to water absorption [58, 59]. Also, the PA12 increases the viscosity of the paste. Therefore, the 10 wt% material is more prone to collapse under the effect of its own weight.

Results in Table 5 also show a significant role of a_n on the results. In particular, the measured diameter decreases while increasing the nozzle acceleration. Finally, the diameter depends on the position within the extruded line. Specifically, the diameter is maximum in the central region and minimum at the ends of the deposited lines.

3.1.2. Standard deviation

The results of the ANOVA performed on the standard deviation values are reported in Table 6. The adjusted R^2 of the GLM was equal to 66.93%. The normal probability plot for standardised residuals is shown in Figure 7. The p-value and KS coefficient calculated by means of the KS normality test were equal to 0.087 and 0.044, respectively. It is thus possible to validate also in this case the hypothesis of normally distributed residuals.

Table 6: ANOVA on the standard deviation of points. Table by authors.

Parameter	DF	Adj SS	Adj. MS	F-value	P-value
v_n	2	1.28×10^{-3}	6.40×10^{-4}	9.20	0.00
wt% PA12	3	1.34×10^{-2}	4.47×10^{-3}	6.42×10	0.00
Position	4.00	3.65×10^{-2}	9.12×10^{-3}	1.31×10^{2}	0.00
a_n	1	8.70×10^{-5}	8.70×10^{-5}	1.25	2.64×10^{-1}

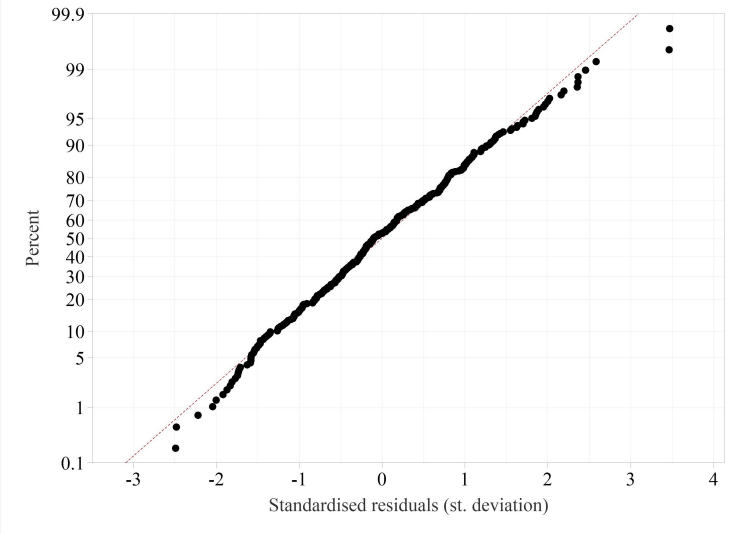

Figure 7: Normal probability plot for standardised residuals of ANOVA on standard deviations. Figure by authors.

The results in Table 6 show that the standard deviation, and thus the geometrical accuracy, is mainly affected by the PA12 wt% and the position within the deposited line. The influence of these parameters can be seen in Figure 8, which shows the plot of the main effects on standard deviation.

By observing Figure 8, it can be noticed that the compositions with 10 wt% and 40 wt% of PA12 exhibit the maximum standard deviation. This effect is arguably attributable to the unstable behaviour of these compositions during extrusion. Specifically, the high water content in the 10 wt% material (already discussed in section 3.1.1) may determine the separation of phases. In the case of

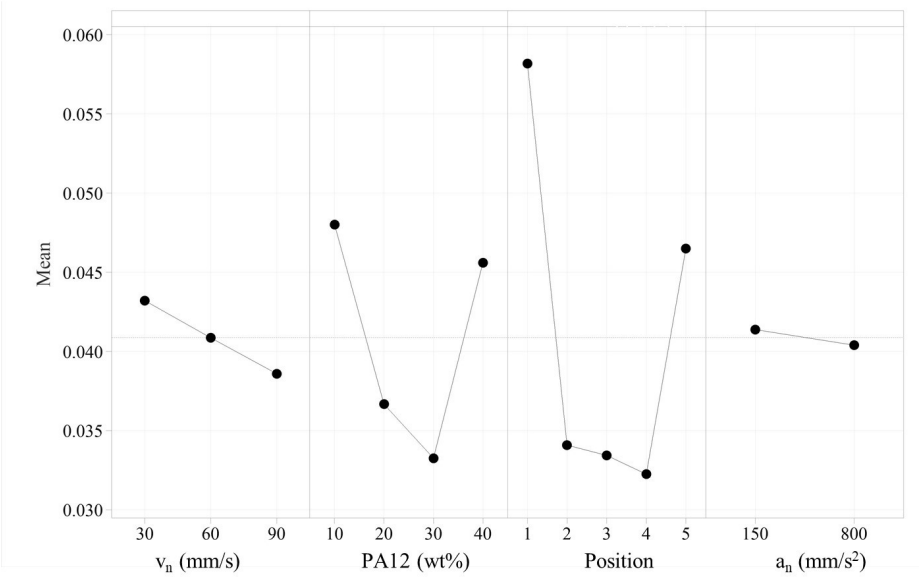

Figure 8: Main effects plot for standard deviation. Figure by authors.

the 40 wt% mixture, the variation is arguably attributable to the high content of the polymer, which might determine a non-homogeneous blend between powder and clay paste.

The shape error is maximum at the ends of the deposited lines, namely positions 1 and 5. This can be explained if considering the material accumulation within the second extruder and the changes in velocity occurring at the ends of the path.

3.2. Dimensional accuracy

The measurements of dimensional accuracy are reported in supplementary Tables 1-4. As shown in Figure 3, the bounding box of each specimen in the cartesian coordinate system is equal to $50mm \times 50mm \times 50mm$. Also, the internal dimensions L_xci and L_{yci} of the hollow cube are both equal to $34mm$. Since the dimensional accuracy of 3D printed parts may significantly depend on the direction, a preliminary analysis of measurements has been performed to understand which dimensions can be considered together and which must be

analysed independently. Specifically, two-sample t-tests [52] have been carried out to compare the dimensions of each specimen having the same nominal value. The results of these analyses are summarised in Table 7.

Table 7: Results of T-tests on measured values of nominally equal dimensions. Table by authors.

Specimen	Null hypothesis	t-Student	p-value
Full cube	$L_{xc} = L_{yc}$	0.6703	0.5049
Full cube	$L_{xc} = L_{zc}$	9.5521	< 0.0001
Full cube	$L_{yc} = L_{zc}$	8.7769	< 0.0001
Hollow cube	$L_{xce} = L_{yce}$	0.5468	0.5862
Hollow cube	$L_{xc} = L_{zc}$	5.3497	< 0.0001
Hollow cube	$L_{yc} = L_{zc}$	4.648	< 0.0001
Hollow cube	$L_{xci} = L_{yci}$	1.4482	0.152
Hollow cube	$L_{xci} = L_{zci}$	110.1464	< 0.0001
Hollow cube	$L_{yci} = L_{zci}$	108.5768	< 0.0001
Full cylinder	$D_c = H_{zc}$	8.5995	< 0.0001
Hollow cylinder	$D_{ce} = H_{zce}$	6.1364	< 0.0001
Hollow cylinder	$D_{ci} = H_{zci}$	104.4002	0.5862

As can be seen in Table 7, the tests between dimensions along the Z direction and those along the X and Y directions return p-values less than 0.0001. This allows for rejecting the null hypothesis, i.e. the vertical dimensions (i.e. those along the Z-axis) are statistically different from others. The accuracy results in this direction are discussed in Section 3.2.1.

On the other hand, p-values higher than 0.05 are found when comparing dimensions along the X and Y directions. This finding suggests that the dimensional accuracy does not depend on the orientation in the XY plane. For this reason, the dimensions along the X and Y directions will be analysed together in Section 3.2.2.

3.2.1. Accuracy along the Z-axis

By looking at the parts after the printing process (Figure 9), a severe slumping can be clearly observed on those with higher PA12 content. This result is consistent with findings by [36] and supports the idea that most of the dimensional error occurring during printing is due to the collapse of the part under its own weight [60]. This is more evident when increasing the percentage of PA12 since, being the water content constant, the amount of solid clay decreases. It is worth mentioning that this phenomenon is more evident in this study than it was in [36] due to the larger dimensions of the investigated parts. The slumping at the green state for high PA12 wt% was observed in all the investigated geometries, as can be seen in Figure 10, which shows the measured height of each specimen. This height corresponds to the dimensions L_{zc}, L_{zce}, H_{zc} and H_{zce} for the full cube, the hollow cube, the full cylinder and the hollow cylinder, respectively (see also Figure 3).

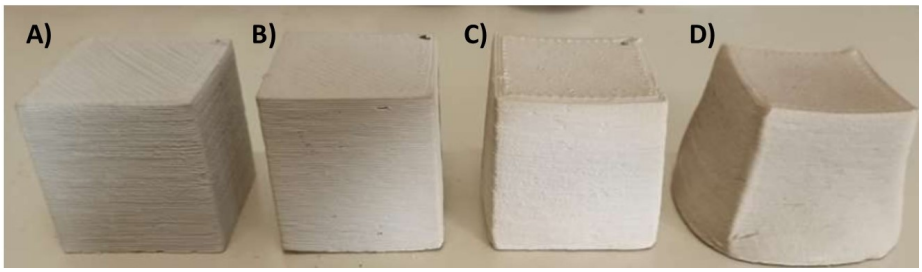

Figure 9: Picture of the specimens after printing. A) 10 wt% PA12, B) 20 wt% PA12, C) 30 wt% PA12, D) 40 wt% PA12. Figure by authors.

3.2.2. Accuracy in the XY plane

In order to quantify the distortion induced by each step of the post-processing cycle, the relative error with the previous operation is calculated as in Equation 1 [36]:

$$E_{r,\%} = \frac{L_{i-1} - L_i}{L_{i-1}} \times 100 \tag{1}$$

where L_i is the value of dimension L at the generic i-th step.

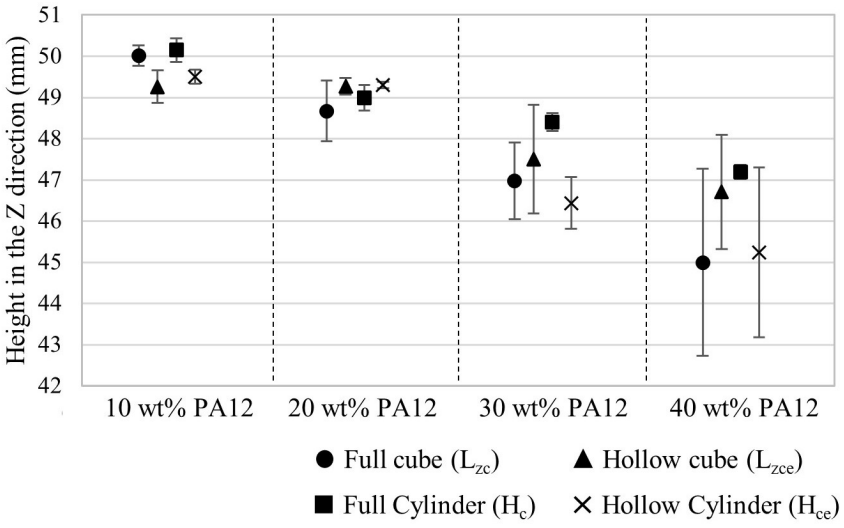

Figure 10: Height of the different specimens according to the content of PA12. Figure by authors.

Figure 11 shows the relative errors for dimensions in the XY plane. These dimensions are L_{xc} and L_{yc} for the full cube, L_{xce} and L_{yce} for the full cube, D_c for the full cylinder and D_{ce} for the hollow cylinder.

As can be observed in Figure 11, the dimensional error after deposition (wet) is higher for mixtures with high percentages of powder. This is coherent with the results found for Z dimensions. The collapse due to the lower self-supporting capability of the material is thus responsible also for a loss of accuracy in the XY plane.

An opposite trend is observed after the drying phase. Specifically, the specimens with more PA12 content show less shrinkage in this phase. This is likely attributable to the lower water absorption of the polymer if compared to clay. The results also show that the effect of melting on dimensional error is marginal if compared to those of previous phases.

These findings are consistent with those of [36]. Nevertheless, a far more clear relation between the PA12 content and the dimensional error is observed in this study. This is arguably due to the larger dimension of specimens, which

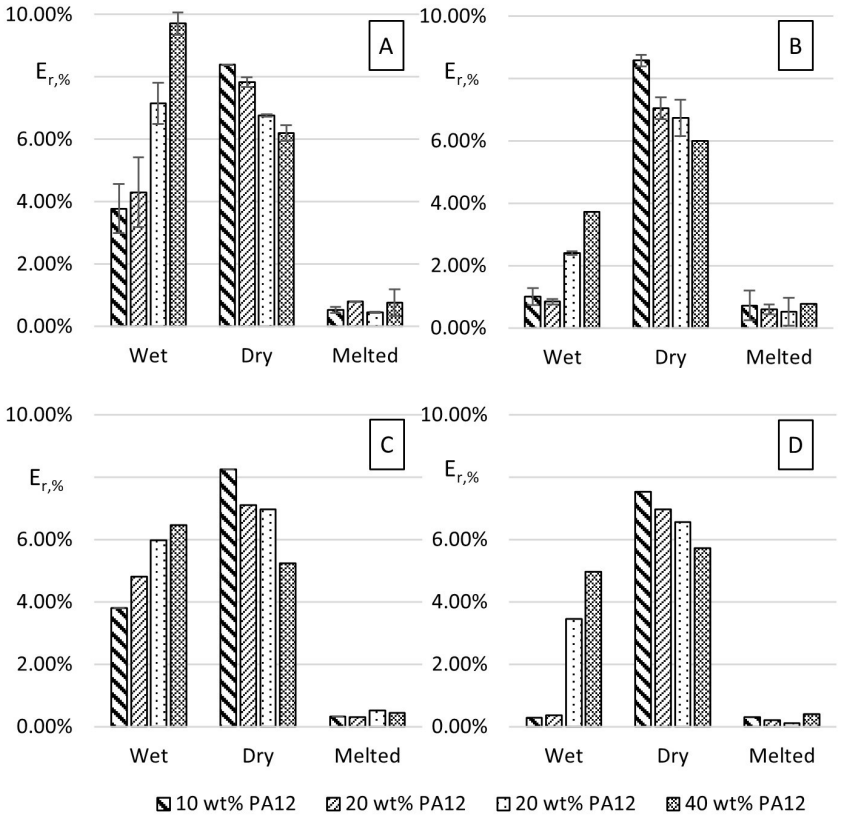

Figure 11: Relative error $E_{r,\%}$observed in the XY plane for the four geometries: A) full cube (L_{xc}, L_{yc}), B) hollow cube (L_{xce}, L_{yce}), C) full cylinder (D_c), D) hollow cylinder (D_{ce}). Figure by authors.

allows for a better observation of the effects on dimensional accuracy.

One significant difference with previous findings is that the dimensional error observed at the green state is highly more relevant in the present study. This suggests that the dimensional error after printing is mainly attributable to the collapse of geometries under the effects of material weight. On the other hand, the per cent error occurring during drying is related to the material composition and does not show significant differences varying the dimensions of parts. This idea is also supported by the fact that the highest errors are observed in the case of full geometries, namely A and C, in which more weight acts on the parts.

3.3. Impact resistance

Table 8 summarises the actual weight and dimensions of the specimens used for impact tests.

Table 8: Actual weight and dimensions of the manufactured specimens. Table by authors.

PA12 content	Weight (g)	Length (mm)	Height (mm)	Depth (mm)
0%	272.6 ± 4.1	147.1 ± 0.7	99.5 ± 0.7	10.1 ± 0.2
10%	235.8 ± 9.4	148.9 ± 0.7	100.3 ± 0.4	10.0 ± 0.2
20%	209.8 ± 5.8	149.7 ± 0.4	100.2 ± 0.3	10.3 ± 0.1
30%	184.8 ± 9.5	150.1 ± 0.4	100.1 ± 0.2	10.3 ± 0.2
40%	155 ± 14.0	149.0 ± 0.8	100.3 ± 0.9	10.3 ± 0.2

Figure 12 shows the force (F) versus displacement (z) diagrams obtained for each material composition. The highest point of these graphs represents the maximum force, while the area under each line is equal to the absorbed energy. These values are also reported in Table 9.

Table 9: Maximum force and absorbed energy of specimens according to the PA12 content. Table by authors.

wt% PA12	Maximum force (kN)	Absorbed energy (J)
0%	0.344 ± 0.049	0.758 ± 0.131
10%	1.379 ± 0.147	2.896 ± 0.441
20%	1.953 ± 0.28	4.458 ± 0.286
30%	1.981 ± 0.204	4.746 ± 0.252
40%	1.558 ± 0.282	4.553 ± 0.992

By observing the results in Figure 12 and Table 9, it is possible to notice that the specimens made of pure clay show the lowest impact resistance. Specifically, the maximum force and the absorbed energy increase with the content of PA12 until the 30 wt% is reached. This finding can be explained by considering the higher elasticity of polyamide infiltrating between the clay grains. The resilience of these specimens determines also a more pronounced deformation

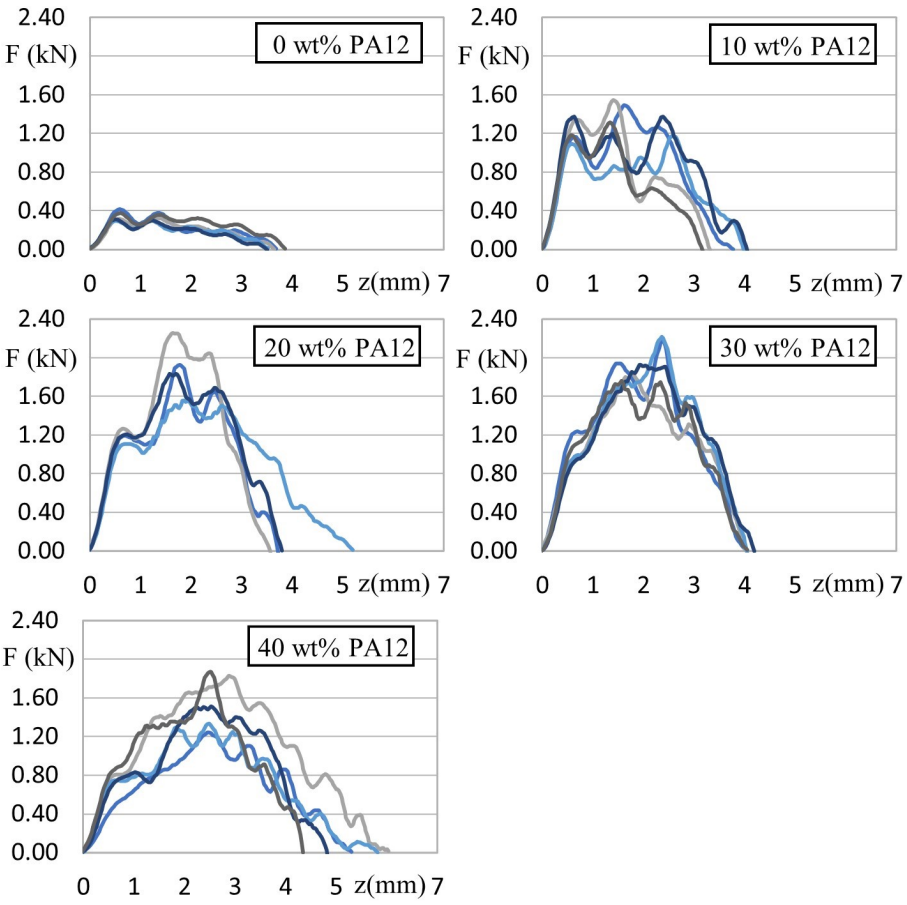

Figure 12: Variation of force in time during drop weight tests for various percentages of PA12. Figure by authors.

before breaking, as demonstrated by the higher deformation before breaking shown in Figure 12. Accordingly, a sharp difference can be observed in the fracture mode of the specimens, as shown by the picture in Figure 13. Looking at Figure 13 a), it is possible to notice that the impactor passed through the specimens. On the other hand, the specimen in Figure 13 b) shows a brittle fracture with cracks connecting the impact region with the four clamps.

Interestingly, the maximum force and absorbed energy are observed to decrease in the 40 wt% PA12 paste. This may be explained by the different

Figure 13: Picture of fractured specimens after the drop weight test. a) 0 wt% PA12 and b) 30 wt% PA12

densities of specimens at the end of the post-processing. In fact, [36] showed that the melting of the polymeric phase is responsible for porosities within the final parts. Arguably, when the powder content is too high, the detrimental effect of these voids surpasses the benefits provided by the PA12.

Another possible explanation for the decrease in resistance is that the excessive amount of polymer determines a non-homogenous blend with the clay. This hypothesis is consistent with the results of deposition tests presented in section 3.1. As a consequence, the part may contain randomly distributed regions with lower impact resistance due to a higher content of clay. This idea is supported by the standard deviation of absorbed energy observed in Table 9 for the 40 wt% mixture, which is significantly higher than all the other compositions.

Most likely, a combination of these two effects contributes to the reduction of impact resistance. Future work is planned to study these phenomena more in-depth. The most important aspect of these findings is that an optimal composition maximising impact resistance exists for a PA12 content between 20 wt% and 40 wt%.

4. Conclusions

The research presented in this paper contributed to providing a more in-depth insight into the 3D printing of clay paste enhanced by PA12 powder.

Firstly, the factors influential to deposition have been investigated. Then, the results of previous studies concerning part accuracy have been extended to larger dimensions. Finally, for the first time, the mechanical properties of these materials have been observed by impact tests. The main findings can be summarised as follows:

- The PA12 content, deposition speed and acceleration contribute to determining the width and regularity of the deposited lines. These outputs change significantly at the beginning and end of the deposition,
- Material with 10 wt% PA12 shows larger lines since it is more prone to collapse under its own weight. Lines deposited with 10 wt% and 40 wt% PA12 mixtures exhibit irregular shapes due to the separation of phase,
- For high dimensions, the effect of material weight at the green state significantly affects the dimensional accuracy both along the Z-axis and in the XY plane,
- The effect of weight on dimensional accuracy is more pronounced for specimens with higher content of PA12,
- PA12 positively affects dimensional accuracy during post-processing since it reduces the shrinkage provoked by drying,
- PA12 determines a tremendous increase in the impact resistance of manufactured parts if compared to pure clay,
- A decrease in the maximum force and absorbed energy can be observed on benchmarks with 40 wt% PA12.

Overall, the results suggest that a percentage of PA12 around 20-30% should be preferred for the 3D printing process. In fact, these percentages showed the highest repeatability of deposited lines. As far as dimensional accuracy is concerned, these compositions exhibited a good compromise between loss of resistance at the green state and shrinkage reduction during drying. Finally,

the 30% mixture exhibited the maximum resistance to impacts. Future research should be carried out around these compositions investigating the physical and mechanical properties of the printed material. Also, further studies are needed to compare the environmental and economic impacts of this novel technique to those of current practices used to dispose of scrap powder.

Acknowledgments

Financed by the European Union - NextGenerationEU (National Sustainable Mobility Center CN00000023, Italian Ministry of University and Research Decree n. 1033 - 17/06/2022, Spoke 11 - Innovative Materials & Lightweighting). The opinions expressed are those of the authors only and should not be considered as representative of the European Union or the European Commission's official position. Neither the European Union nor the European Commission can be held responsible for them.

References

[1] C. R. Deckard, Method and apparatus for producing parts by selective sintering (1989).

[2] A. Awad, F. Fina, A. Goyanes, S. Gaisford, A. W. Basit, 3D printing: Principles and pharmaceutical applications of selective laser sintering, International Journal of Pharmaceutics 586 (July) (2020) 119594. doi:10.1016/j.ijpharm.2020.119594.
URL https://doi.org/10.1016/j.ijpharm.2020.119594

[3] N. A. Charoo, S. F. Barakh Ali, E. M. Mohamed, M. A. Kuttolamadom, T. Ozkan, M. A. Khan, Z. Rahman, Selective laser sintering 3D printing–an overview of the technology and pharmaceutical applications, Drug Development and Industrial Pharmacy 46 (6) (2020) 869–877. doi:10.1080/03639045.2020.1764027.
URL https://doi.org/10.1080/03639045.2020.1764027

[4] F. Lupone, E. Padovano, F. Casamento, C. Badini, Process phenomena and material properties in selective laser sintering of polymers: A review, Materials 15 (1) (2022). doi:10.3390/ma15010183.

[5] Y. Wang, Z. Xu, D. Wu, J. Bai, Current status and prospects of polymer powder 3D printing technologies, Materials 13 (10) (2020). doi:10.3390/ma13102406.

[6] N. Hopkinson, P. Erasenthiran, High speed sintering-early research into a new rapid manufacturing process, in: Solid Freeform Fabrication Symposium, 2004, pp. 312–320.

[7] A. Ellis, High Speed Sintering : The Next Generation of Manufacturing, Nanomaterials for 2D and 3D Printing (2017) 107–118.

[8] B. Asiabanpour, B. Khoshnevis, K. Palmer, Advancements in the selective inhibition sintering process development, Virtual and Physical Prototyping 1 (1) (2006) 43–52. doi:10.1080/17452750500289910.

[9] P. Arunkumar, E. Balasubramanian, U. Chandrasekhar, Thermo Mechanical Modeling of Selective Inhibition Sintered Thermoplastic Parts, Applied Mechanics and Materials 813-814 (2015) 791–795. doi:10.4028/www.scientific.net/amm.813-814.791.

[10] H. J. O'Connor, A. N. Dickson, D. P. Dowling, Evaluation of the mechanical performance of polymer parts fabricated using a production scale multi jet fusion printing process, Additive Manufacturing 22 (May) (2018) 381–387. doi:10.1016/j.addma.2018.05.035.

[11] Z. Xu, Y. Wang, D. Wu, K. P. Ananth, J. Bai, The process and performance comparison of polyamide 12 manufactured by multi jet fusion and selective laser sintering, Journal of Manufacturing Processes 47 (October 2018) (2019) 419–426. doi:10.1016/j.jmapro.2019.07.014.
URL https://doi.org/10.1016/j.jmapro.2019.07.014

[12] S. Rosso, R. Meneghello, L. Biasetto, L. Grigolato, G. Concheri, G. Savio, In-depth comparison of polyamide 12 parts manufactured by Multi Jet Fusion and Selective Laser Sintering, Additive Manufacturing 36 (2020) 101713. doi:10.1016/j.addma.2020.101713.
URL https://doi.org/10.1016/j.addma.2020.101713

[13] Sculpteo, the State Printing of 3D, Tech. rep. (2021).

[14] Grand View Research, 3D Printing Market Size, Share & Trends Analysis Report By Component, By Printer Type (Desktop, Industrial), By Technology, By Software, By Application, By Vertical, By Material, By Region, And Segment Forecasts, 2021 - 2028, Tech. rep. (2021).
URL https://www.grandviewresearch.com/industry-analysis/3d-printing-industry-analysis/methodology

[15] Z. Liu, Q. Jiang, F. Ning, H. Kim, W. Cong, C. Xu, H. C. Zhang, Investigation of energy requirements and environmental performance for additive manufacturing processes, Sustainability (Switzerland) 10 (10) (2018). doi:10.3390/su10103606.

[16] F. L. Garcia, V. A. d. S. Moris, A. O. Nunes, D. A. L. Silva, Environmental performance of additive manufacturing process – an overview, Rapid Prototyping Journal 24 (7) (2018) 1166–1177. doi:10.1108/RPJ-05-2017-0108.

[17] F. Fruggiero, A. Lambiase, R. Bonito, M. Fera, The load of sustainability for Additive Manufacturing processes, Procedia Manufacturing 41 (2019) 375–382. doi:10.1016/j.promfg.2019.09.022.
URL https://doi.org/10.1016/j.promfg.2019.09.022

[18] A. Martínez, A. Ibáñez, A. Sánchez, M. A. León, Comparison of aged polyamide powders for selective laser sintering, AIP Conference Proceedings 1431 (1) (2012) 5–13. doi:10.1063/1.4707544.

[19] F. Sillani, R. G. Kleijnen, M. Vetterli, M. Schmid, K. Wegener, Selective laser sintering and multi jet fusion: Process-induced modification of the

raw materials and analyses of parts performance, Additive Manufacturing 27 (November 2018) (2019) 32–41. doi:10.1016/j.addma.2019.02.004.
URL https://doi.org/10.1016/j.addma.2019.02.004

[20] K. Wudy, D. Drummer, Aging effects of polyamide 12 in selective laser sintering: Molecular weight distribution and thermal properties, Additive Manufacturing 25 (November 2018) (2019) 1–9. doi:10.1016/j.addma.2018.11.007.
URL https://doi.org/10.1016/j.addma.2018.11.007

[21] P. Chen, J. Su, H. Wang, L. Yang, M. Li, Z. Li, J. Liu, S. Wen, Y. Zhou, C. Yan, Y. Shi, Aging mechanism of polyetheretherketone powder during layer-wise infrared radiation of high-temperature laser powder bed fusion, Materials and Design 213 (2022) 110348. doi:10.1016/j.matdes.2021.110348.
URL https://doi.org/10.1016/j.matdes.2021.110348

[22] K. Dotchev, W. Yusoff, Recycling of polyamide 12 based powders in the laser sintering process, Rapid Prototyping Journal 15 (3) (2009) 192–203. doi:10.1108/13552540910960299.

[23] J. Riedelbauch, D. Rietzel, G. Witt, Analysis of material aging and the influence on the mechanical properties of polyamide 12 in the Multi Jet Fusion process, Additive Manufacturing 27 (October 2018) (2019) 259–266. doi:10.1016/j.addma.2019.03.002.
URL https://doi.org/10.1016/j.addma.2019.03.002

[24] D. T. Pham, K. D. Dotchev, W. A. Y. Yusoff, Deterioration of polyamide powder properties in the laser sintering process, Proceedings of the Institution of Mechanical Engineers, Part C: Journal of Mechanical Engineering Science 222 (11) (2008) 2163–2176. doi:10.1243/09544062JMES839.

[25] S. Josupeit, J. Lohn, E. Hermann, M. Gessler, S. Tenbrink, H. J. Schmid, Material properties of laser sintered polyamide 12 as function of build cycles using low refresh rates, Proceedings - 26th Annual International Solid

Freeform Fabrication Symposium - An Additive Manufacturing Conference, SFF 2015 (2020) 540–548.

[26] P. Mägi, A. Krumme, M. Pohlak, Material recycling and improvement issues in additive manufacturing, Proceedings of the International Conference of DAAAM Baltic 2015-Janua (May) (2015) 63–68.

[27] S. Kumar, A. Czekanski, Development of filaments using selective laser sintering waste powder, Journal of Cleaner Production 165 (2017) 1188–1196. doi:10.1016/j.jclepro.2017.07.202.
URL http://dx.doi.org/10.1016/j.jclepro.2017.07.202

[28] L. Wang, A. Kiziltas, D. F. Mielewski, E. C. Lee, D. J. Gardner, Closed-loop recycling of polyamide12 powder from selective laser sintering into sustainable composites, Journal of Cleaner Production 195 (2018) 765–772. doi:10.1016/j.jclepro.2018.05.235.
URL https://doi.org/10.1016/j.jclepro.2018.05.235

[29] M. Uddin, D. Williams, A. Blencowe, Recycling of selective laser sintering waste Nylon powders into fused filament fabrication parts reinforced with Mg particles, Polymers 13 (13) (2021). doi:10.3390/polym13132046.

[30] L. Feng, Y. Wang, Q. Wei, PA12 powder recycled from SLS for FDM, Polymers 11 (4) (2019). doi:10.3390/polym11040727.

[31] J. Kawabata, G. Matsuba, K. Nishida, R. Inoue, T. Kanaya, Melt memory effects on recrystallization of polyamide 6 revealed by depolarized light scattering and small-angle X-ray scattering, Journal of Applied Polymer Science 122 (3) (2011) 1913–1920.

[32] N. Vidakis, M. Petousis, L. Tzounis, A. Maniadi, E. Velidakis, N. Mountakis, J. D. Kechagias, Sustainable additive manufacturing: Mechanical response of polyamide 12 over multiple recycling processes, Materials 14 (2) (2021) 1–15. doi:10.3390/ma14020466.

[33] C. Cardona, A. H. Curdes, A. J. Isaacs, Effects of Filament Diameter Tolerances in Fused Filament Fabrication, IU Journal of Undergraduate Research 2 (1) (2016) 44–47. doi:10.14434/iujur.v2i1.20917.

[34] E. Gkartzou, E. P. Koumoulos, C. A. Charitidis, Production and 3D printing processing of bio-based thermoplastic filament, Manufacturing Review 4 (2017). doi:10.1051/mfreview/2016020.

[35] B. Peeters, N. Kiratli, J. Semeijn, A barrier analysis for distributed recycling of 3D printing waste: Taking the maker movement perspective, Journal of Cleaner Production 241 (2019) 118313. doi:10.1016/j.jclepro.2019.118313.
URL https://doi.org/10.1016/j.jclepro.2019.118313

[36] M. Mele, M. Ricciarelli, G. Campana, 3D printing of clay paste enhanced by scrap polymer from powder bed processes, Rapid Prototyping Journal (2021).

[37] Y. Xing, Y. Zhou, X. Yan, H. Zhao, W. Liu, J. Jiang, L. Lu, Shell thickening for extrusion-based ceramics printing, Computers and Graphics (Pergamon) 97 (2021) 160–169. doi:10.1016/j.cag.2021.04.031.
URL https://doi.org/10.1016/j.cag.2021.04.031

[38] A. Wolf, P. L. Rosendahl, U. Knaack, Additive manufacturing of clay and ceramic building components, Automation in Construction 133 (September 2021) (2022) 103956. doi:10.1016/j.autcon.2021.103956.
URL https://doi.org/10.1016/j.autcon.2021.103956

[39] P. Biswas, S. Mamatha, K. Varghese, R. Johnson, R. Vijay, R. Kumar, 3D printing of high surface area ceramic honeycombs substrates and comparative evaluation for treatment of sewage in Phytorid application, Journal of Water Process Engineering 37 (June) (2020) 101503. doi:10.1016/j.jwpe.2020.101503.
URL https://doi.org/10.1016/j.jwpe.2020.101503

[40] V. Sangiorgio, F. Parisi, F. Fieni, N. Parisi, The New Boundaries of 3D-Printed Clay Bricks Design: Printability of Complex Internal Geometries, Sustainability (Switzerland) 14 (2) (2022). doi:10.3390/su14020598.

[41] A. Ruscitti, C. Tapia, N. M. Rendtorff, A review on additive manufacturing of ceramic materials based on extrusion processes of clay pastes, Ceramica 66 (380) (2020) 354–366. doi:10.1590/0366-69132020663802918.

[42] F. Zhong, W. Liu, Y. Zhou, X. Yan, Y. Wan, L. Lu, Ceramic 3D printed sweeping surfaces, Computers and Graphics (Pergamon) 90 (2020) 108–115. doi:10.1016/j.cag.2020.05.007.
URL https://doi.org/10.1016/j.cag.2020.05.007

[43] E. R. Ramírez, S. A. H. Moreno, E. T. Díaz, N. P. Burgos, G. G. Moreno-Contreras, Design of a Clay Extrusion System for Low Cost 3D Printing, ARPN Journal of Engineering and Applied Sciences 16 (12) (2021) 1235–1239.

[44] M. Jemberu, F. Shemsu, M. Gopal, Investigation of different clay compositions and additives for energy- efficient and impact-resistant Injera baking pan, Materials Today: Proceedings (xxxx) (2023). doi:10.1016/j.matpr.2023.02.035.
URL https://doi.org/10.1016/j.matpr.2023.02.035

[45] S. S. Ray, Recent trends and future outlooks in the field of clay-containing polymer nanocomposites, Macromolecular Chemistry and Physics 215 (12) (2014) 1162–1179. doi:10.1002/macp.201400069.

[46] F. Ali, H. Ullah, Z. Ali, F. Rahim, F. Khan, Z. Ur Rehman, Polymer-clay Nanocomposites, Preparations and Current Applications: A Review, Current Nanomaterials 1 (2) (2016) 83–95. doi:10.2174/2405461501666160625080118.

[47] M. Tanniru, Q. Yuan, R. D. Misra, On significant retention of impact strength in clay-reinforced high-density polyethylene (HDPE) nanocom-

posites, Polymer 47 (6) (2006) 2133–2146. doi:10.1016/j.polymer.2006.01.063.

[48] K. Zdiri, A. Elamri, M. Hamdaoui, Advances in Thermal and Mechanical Behaviors of PP/Clay Nanocomposites, Polymer - Plastics Technology and Engineering 56 (8) (2017) 824–840. doi:10.1080/03602559.2016.1233282.
URL http://dx.doi.org/10.1080/03602559.2016.1233282

[49] C. Deshmane, Q. Yuan, R. S. Perkins, R. D. Misra, On striking variation in impact toughness of polyethylene-clay and polypropylene-clay nanocomposite systems: The effect of clay-polymer interaction, Materials Science and Engineering A 458 (1-2) (2007) 150–157. doi:10.1016/j.msea.2006.12.069.

[50] B. Chen, Polymer-clay nanocomposites: An overview with emphasis on interaction mechanisms, British Ceramic Transactions 103 (6) (2004) 241–249. doi:10.1179/096797804X4592.

[51] HP Development Company L.P., HP Multi Jet Fusion Handbook, Tech. rep. (2019).

[52] D. C. Montgomery, Design and Analysis of Experiments Eighth Edition, 2013. doi:10.1198/tech.2006.s372.

[53] M. T. Lozano, F. B. Haro, A. Ruggiero, J. A. Mendez, Systems of digitalization and processing of anatomical pieces for their three-dimensional reconstruction, ACM International Conference Proceeding Series Part F1322 (2017) 1–5. doi:10.1145/3144826.3145402.

[54] A. Alin, Minitab, Wiley Interdisciplinary Reviews: Computational Statistics 2 (6) (2010) 723–727.

[55] ASTM, Standard Test Method for Measuring the Damage Resistance of a Fiber-reinforced Polymer Matrix Composite to a Drop-weight Impact Event: D7136/D7136M-15, ASTM International, 2015.

[56] H. W. Lilliefors, On the Kolmogorov-Smirnov Test for Normality with Mean and Variance Unknown Author (s): Hubert W . Lilliefors Source : Journal of the American Statistical Association , Vol . 62 , No . 318 (Jun ., 1967), pp . 399- ON THE KOLMOGOROV-SMIRNOV TEST FOR NO, journal of American Statistics 62 (318) (1967) 399–402.

[57] B. Yazici, S. Yolacan, A comparison of various tests of normality, Journal of Statistical Computation and Simulation 77 (2) (2007) 175–183. doi:10.1080/10629360600678310.

[58] C. L. Amorim, R. T. Lopes, R. C. Barroso, J. C. Queiroz, D. B. Alves, C. A. Perez, H. R. Schelin, Effect of clay-water interactions on clay swelling by X-ray diffraction, Nuclear Instruments and Methods in Physics Research, Section A: Accelerators, Spectrometers, Detectors and Associated Equipment 580 (1 SPEC. ISS.) (2007) 768–770. doi:10.1016/j.nima.2007.05.103.

[59] R. L. Anderson, I. Ratcliffe, H. C. Greenwell, P. A. Williams, S. Cliffe, P. V. Coveney, Clay swelling - A challenge in the oilfield, Earth-Science Reviews 98 (3-4) (2010) 201–216. doi:10.1016/j.earscirev.2009.11.003.

[60] S. S. Chan, R. M. Pennings, L. Edwards, G. V. Franks, 3D printing of clay for decorative architectural applications: Effect of solids volume fraction on rheology and printability, Additive Manufacturing 35 (December 2019) (2020) 101335. doi:10.1016/j.addma.2020.101335.
URL https://doi.org/10.1016/j.addma.2020.101335